ISSN 0016-7029, Geochemistry International, 2006, Vol. 44, No. 8, pp. 752–770. © Pleiades Publishing, Inc., 2006.
Original Russian Text © T.Yu. Timina, V.V. Sharygin, A.V. Golovin, 2006, published in Geokhimiya, 2006, No. 8, pp. 814–833.

Melt Evolution during the Crystallization of Basanites of the Tergesh Pipe, Northern Minusinsk Depression

T. Yu. Timina, V. V. Sharygin, and A. V. Golovin

Institute of Mineralogy and Petrography, Siberian Division, Russian Academy of Sciences, pr. akademika Koptyuga 3, Novosibirsk, 630090 Russia

e-mail: timina@gorodok.net, sharygin@uiggm.nsc.ru

Received November 5, 2004

Abstract—In this paper we describe the mineralogy and geochemistry of basanites and melt inclusions in minerals from the Tergesh pipe, northern Minusinsk Depression. The rocks are composed of olivine and clinopyroxene phenocrysts and a groundmass of olivine, clinopyroxene, titanomagnetite, plagioclase, apatite, ilmenite, and glass. Melt inclusions were found only in the olivine and clinopyroxene phenocrysts. Primary melt inclusions in olivine contain glass, rhönite, clinopyroxene, a sulfide globule, and low-density fluid. The phase composition of melt inclusions in clinopyroxene is glass + low-density fluid ± xenogenous magnetite. According to thermometric investigations, the olivine phenocrysts began crystallizing at $T = 1280$–1320°C and $P > 3.5$ kbar, whereas groundmass minerals were formed under near-surface conditions at $T \le 1200$°C. The oxygen fugacity gradually changed during basanite crystallization from oxidizing (NNO) to more reducing conditions (QFM). The investigation of glass compositions (heated and unheated inclusions in phenocrysts and groundmass) showed that the evolution of a basanite melt during its crystallization included mainly an increase in SiO_2, Al_2O_3, and alkalis, while a decrease in femic components, and the melt composition moved gradually toward tephriphonolite and trachyandesite. Geochemical evidence suggests that the primary basanite melt was derived from a mantle source affected by differentiation.

DOI: 10.1134/S0016702906080027

INTRODUCTION

The northern Minusinsk Depression in the southwestern framing of the Siberian craton hosts an area of Late Mesozoic alkali basalt volcanism. This area has been extensively studied since the 1960s in connection with its diamond potential [1–4]. This work demonstrated that the diatremes of the northern Minusinsk Depression are not diamondiferous, in contrast to the kimberlite pipes of the Siberian craton. Subsequent studies focused on mantle xenoliths in the basanites of the depression, whereas the mineralogy and petrography of the basanites received little attention [5–10]. Currently, the mantle xenoliths are comprehensively studied, whereas only fragmentary evidence is available on mineralogy and melt inclusions in minerals from the basalts of the northern Minusinsk Depression [7, 11]. This paper addresses the mineralogy of the basanites and inclusions in their minerals. The goal of our study was the characterization of the chemistry of rock-forming minerals from the basanites and physicochemical conditions of basanite crystallization in the Tergesh pipe.

GEOTECTONIC SETTING OF THE REGION

The Minusinsk intermontane basin is a system of Devonian depressions located between mountain structures of the Kuznetsk Alatau, western Sayan, and eastern Sayan. A peculiar zone of Late Mesozoic alkaline basaltoid volcanism is situated in the northern margin of the Devonian–Carboniferous Minusinsk intermontane basin within the northern Minusinsk Depression. The main tectonic process responsible for the volcanic phenomena was the rifting of the continental lithosphere [8, 9]. Currently, the alkali basalt magmatism is represented mainly by the root systems of volcanic edifices (vent facies, necks, and dikes) [3].

Diatremes and dikes are confined to flexures and faults penetrating deep-base zones, marking weakened zones formed owing to the extensive crushing of the ancient folded base? Five permeable linear zones were distinguished in the northern Minusinsk Depression. Each zone is marked by linearly distributed pipes and parallel dikes [10]. According to the data reported by Luchitskii [1], Kryukov and Kryukova [2], and Kryukov [3, 4], the majority of volcanic pipes and dikes are confined to the periphery of the Kop'evskoe domal uplift, which is located in the central part of the northern Minusinsk Depression. Geographically, two groups of volcanic pipes can be distinguished in the depression: southern (Bele, Krasnoozerskaya, Dzhirim, Chebaldak, Tergesh, Tochil'naya, and Pridorozhnaya) and northern (Kongarovskaya, Tri Brata, Sestra, Klad, Uzhur, Botikha, and others). The Kamyshtinskaya-1 and -2 and Intikol' pipes occur as separate intrusions [10, 11].

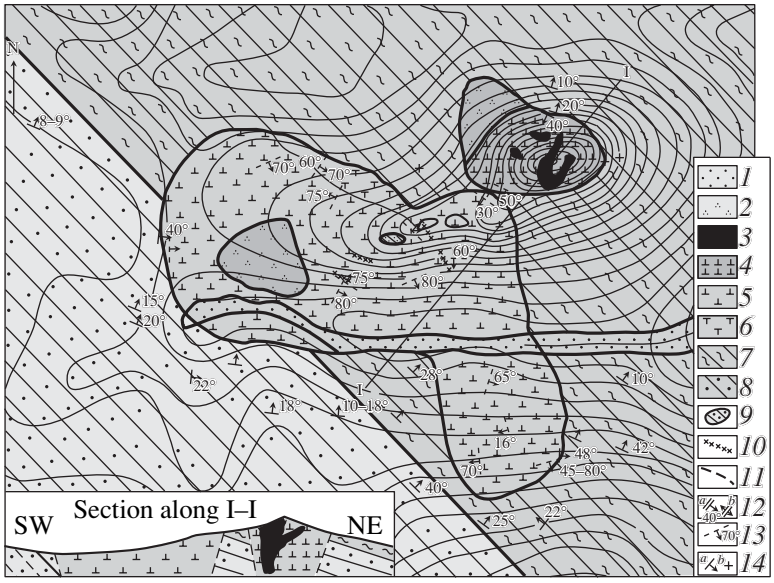

Fig. 1. Geological sketch map of the Tergesh pipe after Kryukov [3]. (*1*) Alluvium, diluvium; (*2*) structural eluvium of breccias; (*3*) basalt; (*4*) eruptive breccia of phase III; (*5*) eruptive breccia of phase II; (*6*) eruptive breccia of phase I; (*7*) mottled red-bed mudstones with interbeds of siltstone, marl, and limestone; (*8*) yellow, gray, and variegated sandstones; (*9*) floating reefs, i.e., large blocks of sandstone in breccia; (*10*) zones of secondary silicification; (*11*) outline of a pipe on the surface according to geological and geophysical data; (*12*) strike and dip of the contact surface of a pipe (*a,* inclined and *b,* vertical); (*13*) strike and dip of a major fracture; and (*14*) strike and dip of sedimentary bedding (*a,* inclined and *b,* vertical).

The basanites intrude the youngest terrigenous deposits of the region of the Devonian and Carboniferous age. Based on this observation, a Late Permian–Triassic age was initially supposed for these volcanic rocks [1, 4]. The first $^{40}K/^{40}Ar$ investigation of the basalts yielded an age of 71–28 Ma for the volcanic pipes (10 analyses), and the majority of pipes lay within the range 65–45 Ma [12]. According to recent $^{39}Ar/^{40}Ar$ datings, the age of basalts from the diatremes ranges from 74 to 81 Ma, and the basanites of the Tergesh pipe are 77 ± 2 Ma old [10, 13, 14].

STRUCTURE OF THE TERGESH PIPE

The structure of the Tergesh pipe is very interesting and can be considered typomorphic in all pipes of the northern Minusinsk Depression [3]. It cuts the Late Devonian sedimentary sequence represented by red-bed calcareous sandstones, mudstones, and minor marls and gravelstones. The pipe is morphologically expressed only in the northeast, where it forms a cone-shaped hill rising 40 m above the surrounding plain. The major portion of the pipe is completely eroded and covered with glacial deposits. The pipe is made up of eruptive breccias of three intrusion phases separately occurring within the pipe and later minor intrusions of basalts forming small (up to 10 m in diameter) stocks with numerous apophyses and dikes [3]. Eruptive breccias are much more abundant than basalts (Fig. 1). They are strongly altered volcaniclastic rocks containing abundant mantle and crustal xenoliths and pyrope xenocrysts [2, 9]. Deep-seated xenoliths are scarce in the basalts. The mantle xenoliths are mainly garnet–spinel and spinel pyroxenites, and spinel and garnet–spinel lherzolites. According to thermobarometric investigations, the garnet-bearing xenoliths of the Tergesh pipe are the deepest mantle rocks detected in the basalts of the northern Minusinsk Depression [10, 15].

ANALYTICAL METHODS

The bulk compositions of basanites from the Tergesh pipe were determined by X-ray fluorescence analysis at the Joint Institute of Geology, Geophysics, and Mineralogy, Siberian Division, Russian Academy of Sciences, Novosibirsk. Trace elements in the rocks were analyzed by the SR–XRF technique at the Institute of Nuclear Physics, Siberian Division, Russian Academy of Sciences, Novosibirsk. The trace-element compositions and water contents of glasses from the basanite groundmass were measured with an ion microprobe at the Institute of Microelectronics, Russian Academy of Sciences, Yaroslavl.

Thermometric investigations of melt inclusions in minerals were carried out using two techniques: with and without visual inspection. The investigations of inclusions with visual observation were conducted using a heating stage with an argon atmosphere designed at the Vernadsky Institute of Geochemistry and Analytical Chemistry, Russian Academy of Sciences. Olivine grains free of groundmass fragments

were selected for these experiments. This method allowed for determining the temperatures of daughter phase disappearance and homogenization of inclusions. High-temperature experiments without visual inspection were conducted with inclusions in olivine only. For these experiments, pure olivine grains without groundmass and any signs of secondary alteration were separated from three fractions of crushed rock (>0.5 mm, 0.5–0.25 mm, and 0.25–0.15 mm; samples Tsh-77 and Tsh-78). The separated grains were loaded into a ceramic or graphite capsule and placed into a heating stage with an argon atmosphere designed at the Institute of Mineralogy and Petrography, Siberian Division, Russian Academy of Sciences [16]. The grains were heated to temperatures of 1280–1320°C corresponding to the homogenization range of inclusions and exposed to the experimental temperature for 20 min. The heating was conducted without visual observation and the grains were quenched by rapid cooling. The heated samples were polished with diamond pastes to bring the inclusions to the surface for subsequent microprobe examinations.

The minerals of basanites and melt inclusions (heated and unheated glasses, and daughter minerals) were analyzed on a Camebax-micro electron microprobe at the Joint Institute of Geology, Geophysics, and Mineralogy, Siberian Division, Russian Academy of Sciences, Novosibirsk, in a mode of strong cooling. The measurement conditions were $I = 25–40$ nA, $V = 20$ kV, $t = 30–40$ s, and 2–3 μm beam diameter. Inclusions larger than 10 μm were analyzed. It should be noted that alkali loss (primarily, Na_2O) was observed during glass analysis. This resulted in an underestimation of alkali concentrations and a slight increase in SiO_2 and Al_2O_3 contents. In the case of large inclusions (>20 μm), this effect was occasionally eliminated by glass scanning with the electron beam.

MINERALOGY AND PETROGRAPHY OF ALKALI BASALTS

The Tergesh pipe is composed of basanite-type alkali basalts (Table 1). Their alkaline character is reflected in the nepheline-normative composition (up to 10% nepheline) and the lack of modal and normative orthopyroxene [7]. The rocks show massive structures and fine- to medium-grained porphyritic textures. Both glassy and holocrystalline basanite varieties were found. Glassy basanites are common in the vent of the pipe. Olivine and, occasionally, zoned clinopyroxene occur as phenocrysts (up to 10 vol %). The groundmass consists of olivine, clinopyroxene, calcic plagioclase, Ti-magnetite, F-apatite, ilmenite, and glass. In addition to glass (occasionally, up to 15 vol %), the groundmass contains a fine-grained aggregate produced by the devitrification of glass. The holocrystalline basanites also contain potassium feldspar. The rocks show weak secondary alterations represented by the development of serpentine after olivine and analcime after glass.

The olivine phenocrysts are subhedral grains, up to 3 mm in size. Their forsterite content decrease from a core (Fo_{81}) to rim (Fo_{69}). The marginal and central parts of some olivine phenocrysts contain small crystallites of Cr–Al spinel. Olivine occurs in the groundmass as euhedral grains, 100–400 μm in size. Their composition varies from core to rim, from Fo_{72} to Fo_{65}. In general, the evolution of olivine composition in the basanites involves an increase in FeO, CaO, and MnO and a decrease in MgO and NiO (Table 2, Fig. 2).

The clinopyroxene phenocrysts are distinct zoned grains, up to 1 mm in size. Their color changes from a greenish in the central parts to a greenish brown at the rims. The phenocrysts are aluminous Ti-augites with Mg# of 0.69–0.79, 5.6–10.1 wt % Al_2O_3, and 1.7–5.1 wt % TiO_2. The composition of phenocrysts evolves toward an increase in TiO_2, Al_2O_3, and FeO and a decrease in SiO_2, Cr_2O_3, and MgO (Fig. 3). In the groundmass clinopyroxene occurs as isometric and elongated zoned grains, from 100 to 600 μm in size. Their composition is similar to that of the outer zone of the phenocrysts and also corresponds to Ti-augite (Table 3). The outer zones of clinopyroxene phenocrysts and groundmass grains contain small crystallites of plagioclase, apatite, and magnetite. This suggests that clinopyroxene is crystallized together with magnetite, apatite, and plagioclase during late stages.

Plagioclase occurs in the groundmass as elongated grains (up to 300 μm long) of a prismatic habit with polysynthetic twins, and its composition corresponds to $An_{68–51}$. Its SrO content is 0.4–0.6 wt % (Table 4). Plagioclase crystallites from the outer zones of phenocrysts and groundmass were never analyzed because of their small sizes.

Magnetite forms euhedral grains (up to 60 μm) in the groundmass. They have uniform compositions and correspond to Ti-magnetite (wt %): up to 22 TiO_2, 4.4–4.9 Al_2O_3 65–67 FeO_{tot}, 3.5–4.4 MgO, 0.5–0.6 MnO, and negligible contents of other oxides (Table 5). Magnetite crystallites from the outer zones of clinopyroxene phenocrysts are slightly different from the groundmass magnetite in a lower TiO_2 content (20 wt %). No ulvospinel (or ilmenite) exsolution lamellae were found in the magnetite.

Spinel occurs as individual crystallites in the marginal and occasionally in the central zones of olivine phenocrysts. These grains are euhedral, greenish brown in color, and up to 30 μm in size. Their compositions correspond mainly to Cr–Al spinel (14–20 wt % Cr_2O_3, Table 6); Al spinel was occasionally found in the central zones of olivine. The equilibrium values of temperature and oxygen fugacity were calculated from the compositions of coexisting spinels and olivines. The temperature estimates obtained by various thermometers [17, 18] lie mainly within 1100–1300°C, and the oxygen fugacity was 1.5–2.5 orders of magnitude above the QFM buffer.

Table 1. Major- (wt %) and trace-element (ppm) compositions of the basanites of the Tergesh pipe

Component	Tsh-2	Tsh-ssv	Tsh-65	Tsh-66	Tsh-77	Tsh-78	Tsh-77*	B**	OIB
SiO_2	43.96	43.95	46.24	45.73	44.89	44.29	54.14	47.56	49.20
TiO_2	2.45	2.49	1.80	1.89	2.35	2.33	1.17	2.71	2.57
Cr_2O_3	–	–	–	–	–	–	0.01	–	–
Al_2O_3	14.22	14.32	13.52	13.70	14.90	14.62	22.44	14.07	12.80
FeO	11.50	12.51	10.29	10.85	11.25	11.24	6.06	11.90	11.40
MnO	0.17	0.18	0.16	0.17	0.17	0.17	0.11	–	0.17
MgO	8.54	8.90	10.65	10.16	8.28	8.12	0.92	7.31	10.00
CaO	10.05	9.82	8.15	8.53	9.21	9.34	1.65	9.71	10.8
Na_2O	3.50	3.18	3.12	2.99	3.40	3.25	3.28	3.44	2.12
K_2O	1.38	1.88	1.53	1.57	1.15	1.41	3.48	1.30	0.51
P_2O_5	0.77	0.78	0.57	0.59	0.70	0.69	0.73	–	0.25
Cl	–	–	0.35	0.05	0.05	0.24	0.19	–	–
LOI	2.06	0.98	2.93	2.78	2.58	3.41	–	–	–
H_2O	–	–	–	–	–	–	6.04	–	–
F	–	–	–	–	–	–	0.12	–	–
Total	99.90	99.97	100.10	100.15	100.12	100.10	100.34	98.00	99.70
Li	11	10	–	–	–	–	21	–	5.6
Be	2.5	2.7	–	–	–	–	5.2	–	–
B	–	–	–	–	–	–	8.7	–	–
Sc	19	17	–	–	–	–	0.4	–	–
V	169	167	186	165	245	174	32	–	–
Cr	170	181	488	516	279	138	10	200	–
Co	47	47	–	–	–	–	–	48	–
Ni	143	148	145	171	68	65	–	127	–
Cu	67	65	44	58	44	42	–	–	–
Zn	–	–	62	84	85	76	–	–	–
Ga	20	20	6.9	14	14	11	–	–	–
Rb	23	26	14	18	18	17	71	26	31
Sr	1170	1090	602	803	984	945	537	580	660
Y	24	23	16	17	17	15	21	31	29
Zr	207	207	132	1658	388	525	278	295	280
Nb	95	97	59	67	79	74	232	–	48
Mo	5.5	6.8	1.7	3.9	4.2	5.4	–	–	2.4
Sn	–	–	1.9	2.1	3	2.3	–	–	–
Cs	0.4	0.4	<1	13	4.4	16	–	–	0.4
Ba	559	569	415	417	540	535	942	380	350
La	51	52	30	33	44	42	78	34	37
Ce	96	97	65	69	90	82	131	92	80
Pr	11	11	–	–	–	–	–	–	9.7
Nd	43	43	–	–	–	–	41	–	39
Sm	8.5	8.7	–	–	–	–	6.6	–	10
Eu	2.7	2.7	–	–	–	–	1.9	–	3
Tb	1.1	1.0	–	–	–	–	–	–	1.1
Dy	5.1	5.0	–	–	–	–	4.6	–	5.6
Ho	0.1	0.9	–	–	–	–	–	–	1.1
Er	2.1	2.1	–	–	–	–	2.9	–	2.6
Yb	1.5	1.5	–	–	–	–	2.4	2.7	2.2
Lu	0.2	0.2	–	–	–	–	–	–	0.3
Hf	4.5	4.4	–	–	–	–	–	–	7.8
Ta	4.3	4.4	–	–	–	–	–	–	2.7
W	–	–	<1.5	1.7	3.0	<1.5	–	–	–
Pb	4.5	4.0	<1.5	<1.5	<1.5	<1.5	–	–	3.2
Th	6.7	6.6	<1.5	<1.5	<1.5	<1.5	16	–	4.0
U	1.7	1.7	<1.5	<1.5	<1.5	<1.5	5.1	–	1.0

Note: Samples Tsh-2 and Tsh-ssv are after [33]. Tsh-65, Tsh-77, and Tsh-78 (our data), the major elements were analyzed by XRF; Cl and trace elements, by SR XRF; dashes denote something that was not analyzed. Tsh-77*, glass of the basanite groundmass, major oxides were analyzed by electron microprobe; trace elements and H_2O, by ion probe. B**, basalt of the alkali type [19]. OIB is the average composition of ocean island basalts [34].

Table 2. Representative analyses (wt %) of olivine from the basanites of the Tergesh pipe

Component	Large phenocrysts									Groundmass grains				
	Tsh-77		Tsh-78			Tsh-78		Tsh-78		Tsh-77		Tsh-77	Tsh-78	Tsh-78
	c	r	c	m	r	c	r	c	r	c	r	c	c	c
SiO_2	38.78	37.69	38.66	38.43	38.03	38.57	37.79	38.79	38.69	37.88	37.51	37.12	37.24	37.02
FeO	19.79	25.37	19.56	19.70	21.87	19.77	23.12	17.96	19.56	24.13	26.84	27.94	26.21	27.45
MnO	0.31	0.47	0.24	0.27	0.31	0.28	0.38	0.24	0.31	0.42	0.51	0.55	0.50	0.55
MgO	40.46	35.71	40.44	40.12	38.29	40.18	37.19	41.44	40.47	36.73	34.58	33.41	34.59	33.55
CaO	0.35	0.51	0.32	0.27	0.29	0.36	0.45	0.38	0.26	0.38	0.50	0.56	0.45	0.52
NiO	0.14	0.07	0.17	0.14	0.14	0.11	0.06	0.20	0.18	0.13	0.10	0.06	0.09	0.07
Total	99.83	99.82	99.39	98.92	98.92	99.27	98.99	99.01	99.46	99.67	100.04	99.64	99.08	99.16
Mg#	78.46	71.50	78.65	78.40	75.73	78.36	74.14	80.44	78.66	73.06	69.66	68.06	70.16	68.53
Fo	78	71	78	78	75	78	73	80	78	72	69	67	69	68

Note: All iron is given as FeO; Al_2O_3, Cr_2O_3, and TiO_2 are below detection limits; c, m, and r are the core, middle, and rim of crystals. Mg# = Mg/(Mg + Fe).

Minor amounts of apatite occur in the groundmass as elongated crystals, up to 100 μm long. Its composition corresponds to F-apatite (Table 7) with minor SiO_2 (up to 0.6 wt %), SrO (up to 0.5 wt %), and Cl (up to 0.4 wt %).

Ilmenite forms thin laths in a fine-grained crystalline aggregate, and was only qualitatively analyzed because of its small size.

The composition of groundmass glass corresponds to trachyandesite and andesite (Tables 1, 7; 51.1–

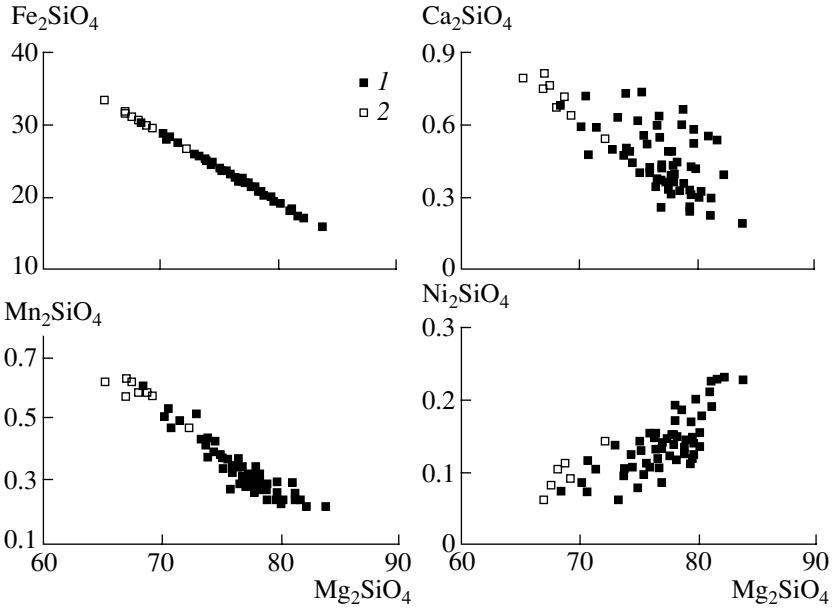

Fig. 2. Variations in olivine composition from the basanites of the Tergesh pipe. (*1*) Olivine phenocrysts and (*2*) microphenocrysts and olivine grains from the groundmass.

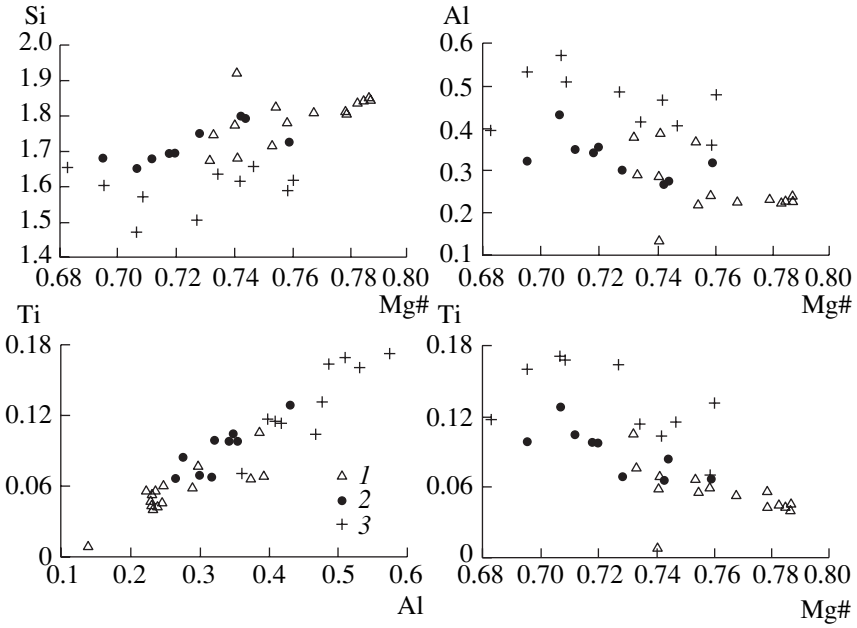

Fig. 3. Variations in the composition of clinopyroxene from the basanite of the Tergesh pipe. (*1*) Zoned phenocrysts, (*2*) clinopyroxene from groundmass, and (*3*) clinopyroxene from melt inclusions in olivine. $Al = Al^{IV} + Al^{VI}$.

55.2 wt % SiO_2 and 4–8 wt % $K_2O + Na_2O$). Ion microprobe analysis revealed considerable water content in the glass (up to 6 wt %). In addition to glass, the groundmass contains a fine-grained crystalline aggre-

Table 3. Representative analyses (wt %) of clinopyroxene from the basanite of the Tergesh pipe

Component	Zoned phenocrysts									Groundmass grains				
	Tsh-78		Tsh-78		Tsh-78		Tsh-77	Tsh-77	Tsh-77	Tsh-78	Tsh-78	Tsh-78	Tsh-78	Tsh-78
	c (1)	r (1)	c (2)	r (1)	c (1)	r(1)	c (1)	c (1)	c (1)	c (1)	c (1)	c (1)	c (1)	c (1)
SiO_2	48.64	41.53	49.58	49.62	46.24	45.12	48.71	48.88	48.10	48.10	46.79	46.03	45.19	44.74
TiO_2	2.03	5.08	1.57	1.69	2.45	2.50	1.94	2.04	2.21	2.36	2.46	2.38	3.46	3.51
Cr_2O_3	0.04	0.05	0.11	0.03	0.05	0.06	0.05	0.02	0.01	0.01	0.01	0.07	0.03	0.01
Al_2O_3	5.37	10.16	5.27	5.60	8.49	8.88	5.28	5.06	5.63	6.06	6.83	7.20	8.05	7.27
FeO	6.91	8.33	6.91	6.71	7.33	7.73	7.35	7.62	7.68	7.61	8.24	7.46	8.10	9.17
MnO	0.15	0.11	0.16	0.16	0.09	0.18	0.14	0.16	0.15	0.13	0.19	0.15	0.10	0.17
MgO	13.59	10.51	14.01	13.86	12.53	12.40	13.59	13.11	13.50	12.30	12.38	13.18	11.68	11.75
CaO	21.49	21.91	20.62	20.60	21.11	21.09	21.81	21.92	22.08	22.55	22.26	22.01	22.49	22.05
Na_2O	0.71	0.62	0.71	0.76	0.93	0.92	0.57	0.53	0.53	0.66	0.56	0.45	0.55	0.86
Total	98.93	98.30	98.94	99.03	99.23	98.88	99.44	99.34	99.89	99.78	99.72	98.93	99.65	99.54
Fe_2O_3	2.37	4.32	1.36	0.69	4.04	5.66	2.57	1.56	3.48	2.17	3.85	4.66	3.59	6.52
FeO	4.78	4.44	5.68	6.09	3.69	2.64	5.04	6.22	4.55	5.66	4.77	3.26	4.87	3.30
Total	99.17	98.73	99.07	99.10	99.63	99.44	99.70	99.49	100.24	99.99	100.11	99.39	100.01	100.19
Mg#	0.78	0.69	0.79	0.78	0.75	0.74	0.77	0.75	0.76	0.74	0.73	0.76	0.72	0.70
En	40.1	33.0	41.5	41.4	37.9	37.3	39.7	38.6	39.2	36.5	36.6	38.9	35.2	34.6
Fs	11.7	14.9	11.8	11.5	12.6	13.4	12.3	12.9	12.8	12.9	14.0	12.6	13.9	15.4
Wo	48.3	52.1	46.7	47.1	49.5	49.3	48.0	48.5	48.1	50.6	49.4	48.5	50.9	50.0

Note: The number of analyses is shown in parentheses; c and r denote the core and rim of crystals, respectively; FeO and Fe_2O_3 were calculated assuming ideal stoichiometry. $Mg\# = Mg/(Mg + Fe_{tot})$.

Table 4. Representative analyses (wt %) of plagioclase from the groundmass of basanites

Component	Tsh-77	Tsh-77	Tsh-77	Tsh-77	Tsh-77	Tsh-77	Tsh-78	Tsh-78	Tsh-78	Tsh-78	Tsh-78	Tsh-78
SiO_2	52.90	52.04	54.42	51.36	52.25	54.80	52.25	52.07	52.23	52.50	52.58	52.50
TiO_2	0.17	0.14	0.12	0.12	0.13	0.17	0.13	0.13	0.17	0.13	0.13	0.28
Al_2O_3	29.56	30.07	28.12	30.39	29.04	28.26	29.10	29.86	29.95	30.01	29.46	29.10
FeO	0.51	0.54	0.54	0.57	0.79	0.64	0.66	0.54	0.65	0.58	0.61	0.93
MnO	0.00	0.00	0.01	0.00	0.01	0.00	0.02	0.01	0.00	0.02	0.00	0.02
MgO	0.06	0.07	0.05	0.06	0.19	0.10	0.07	0.08	0.06	0.06	0.06	0.16
CaO	11.72	12.62	11.32	13.55	11.97	10.22	12.01	12.27	12.37	12.45	12.03	11.61
BaO	0.06	0.01	0.06	0.00	0.05	0.07	0.07	0.09	0.04	0.06	0.09	0.10
SrO	–	–	–	–	–	–	0.40	0.42	0.44	0.53	0.50	0.56
Na_2O	4.49	3.95	4.76	3.47	4.00	5.12	4.07	4.09	4.08	3.93	4.12	4.10
K_2O	0.34	0.29	0.47	0.23	0.44	0.49	0.36	0.35	0.35	0.34	0.35	0.57
Total	99.81	99.72	99.86	99.74	98.87	99.87	99.15	99.90	100.34	100.61	99.94	99.93
An	57.8	62.6	55.3	66.9	60.9	51.4	59.9	60.3	60.6	61.4	59.6	58.9
Ab	40.1	35.4	42.2	31.2	36.9	46.5	36.9	36.4	36.1	35.1	36.9	37.4
Or	2.1	2.0	2.2	1.9	2.2	2.1	3.2	3.3	3.3	3.5	3.5	3.7

Note: All iron is given as FeO; dashes denote something that was not analyzed; *An* – $CaAl_2Si_2O_8$, *Ab* – $NaAlSi_3O_8$, and *Or* – $KAlSi_3O_8$ + $SrAl_2Si_2O_8$ + $BaAl_2Si_2O_8$.

Table 5. Representative analyses (wt %) of titanomagnetite from the groundmass of basanites of the Tergesh pipe

Component	Tsh-78		Tsh-78		Tsh-78	Tsh-78		Tsh-78		Tsh-78		Tsh-78*
	c	r	c	r	c	c	r	c	r	c	r	c
TiO_2	21.38	21.22	21.87	21.93	21.58	21.82	21.68	20.93	21.16	21.53	21.75	20.37
Cr_2O_3	0.18	0.19	0.28	0.24	0.14	0.36	0.29	0.23	0.25	0.29	0.27	0.32
V_2O_3	0.27	0.27	0.23	0.23	0.34	0.30	0.27	0.29	0.27	0.29	0.28	0.31
Al_2O_3	4.61	4.92	4.62	4.61	4.59	4.55	4.48	4.85	4.88	4.82	4.66	5.09
FeO_{tot}	66.23	65.59	65.10	65.91	66.06	65.28	66.20	67.15	66.2	66.13	65.87	66.62
MnO	0.61	0.60	0.59	0.58	0.64	0.64	0.63	0.61	0.63	0.64	0.65	0.62
MgO	3.89	4.22	4.27	4.12	3.85	3.95	3.61	3.62	3.55	4.36	4.13	3.38
NiO	0.10	0.10	0.09	0.06	0.10	0.11	0.10	0.11	0.12	0.12	0.08	0.13
Total	97.28	97.11	97.06	97.68	97.29	97.01	97.26	97.78	97.06	98.18	97.68	96.84
FeO	44.92	44.27	44.72	45.25	45.13	45.08	45.56	45.14	45.18	44.62	45.00	44.70
Fe_2O_3	23.68	23.69	22.64	22.96	23.26	22.45	22.94	24.46	23.36	23.91	23.19	24.36
Total	99.65	99.48	99.33	99.98	99.62	99.26	99.56	100.23	99.40	100.57	100.01	99.28

Note: FeO and Fe_2O_3 were calculated assuming ideal stoichiometry; c and r denote the core and rim of crystals, respectively; Tsh-78* is a magnetite crystallite from the outer zone of a clinopyroxene phenocryst.

Table 6. Representative analyses (wt %) of spinel crystallites from olivine phenocrysts

Component	Tsh-77	Tsh-77	Tsh-78	Tsh-78*	Tsh-78	Tsh-78
	$n = 1$	$n = 1$	$n = 1$	$n = 2$	$n = 2$	$n = 1$
TiO_2	3.26	4.20	7.47	11.46	6.99	1.56
Cr_2O_3	19.83	18.36	14.14	10.97	14.75	1.53
V_2O_3	0.15	0.20	0.20	0.27	0.20	0.15
Al_2O_3	23.04	20.78	15.80	10.05	16.62	55.13
FeO	42.36	44.91	51.81	57.38	49.42	24.18
MnO	0.36	0.37	0.41	0.45	0.33	0.21
MgO	8.40	8.46	7.26	6.12	8.44	16.57
NiO	0.14	0.13	0.13	0.13	0.19	0.25
Total	97.55	97.41	97.22	96.83	96.93	99.58
FeO	24.83	25.23	29.18	33.47	27.00	16.37
Fe_2O_3	19.48	21.87	25.15	26.58	24.91	8.68
Total	99.50	99.60	99.74	99.49	99.42	100.45
*Fo**	73.2	76.9	70.9	71.9	77.0	77.8
T_1, °C	1249	1174	1435	1259	1293	1231
T_2, °C	1104	1123	1223	1253	1226	1001
$\Delta\log(f_{O_2})^{QFM}$	1.90	2.29	2.19	2.44	2.48	1.50

Note: n is the number of analyses; FeO and Fe_2O_3 were calculated assuming ideal stoichiometry; *Fo** is the composition of the host mineral; Tsh-78* is xenogenous spinel from a primary melt inclusion in an olivine phenocryst; T_1 and T_2 are the temperatures calculated using the geothermometers of [17, 18]; and $\Delta\log(f_{O_2})^{QFM}$ is the oxygen fugacity relative to the quartz–fayalite–magnetite buffer.

Table 7. Chemical compositions (wt %) of glass and secondary minerals from the groundmass of basanites of the Tergesh pipe

Component	Tsh-77	Tsh-77	Tsh-77	Tsh-77	Tsh-77	Tsh-77	Tsh-78	Tsh-78	Tsh-78	Tsh-78	Tsh-78	Tsh-78	Tsh-77	Tsh-78	Tsh-78	Tsh-77
	Gl	*Gl*	*Gl*	*Gl*	*Gl*	*Gl*	*Gl*	*Gl*	*Gl*	*Gl*	*Gl*	*Gl*	*Apt*	*Apt*	*Apt*	*Analc*
SiO_2	53.44	54.22	54.30	53.75	52.56	53.56	52.91	52.14	51.10	54.00	55.18	54.15	0.55	0.59	0.61	51.65
TiO_2	0.86	1.14	0.98	0.98	1.25	1.17	1.11	0.87	1.02	1.21	1.12	1.08	0.05	0.02	0.00	0.00
Cr_2O_3	0.01	0.01	0.01	0.00	0.00	0.02	0.00	0.00	0.00	0.00	0.00	0.00	0.00	0.00	0.00	0.00
Al_2O_3	24.42	23.68	23.52	22.71	24.11	23.34	23.63	24.44	22.87	23.67	24.72	22.94	0.00	0.00	0.00	23.17
FeO	4.61	5.31	5.40	5.96	4.92	4.87	5.60	4.09	5.04	5.55	5.05	5.21	0.39	0.37	0.46	0.17
MnO	0.09	0.09	0.11	0.10	0.12	0.10	0.12	0.07	0.06	0.11	0.11	0.11	0.03	0.04	0.02	0.00
MgO	0.76	0.88	0.87	0.76	0.84	0.89	0.79	1.00	0.90	0.88	0.71	0.78	0.22	0.24	0.29	0.03
CaO	1.93	2.08	1.34	1.04	1.57	2.11	1.15	2.75	3.18	1.67	1.36	1.33	53.85	54.16	53.81	0.34
BaO	0.03	0.03	0.04	0.07	0.03	0.03	0.02	0.00	0.02	0.08	0.02	0.05	0.00	0.01	0.01	0.00
SrO	–	–	–	–	–	–	0.00	0.10	0.13	0.00	0.00	0.00	–	0.51	0.50	–
Na_2O	2.02	2.59	1.93	2.00	3.26	2.74	2.23	5.00	6.23	2.80	2.34	3.05	0.14	0.17	0.13	14.54
K_2O	3.29	3.15	2.68	2.65	4.18	2.92	2.41	1.21	1.59	2.36	2.58	2.90	0.00	0.05	0.10	0.08
P_2O_5	0.68	0.63	0.65	0.64	0.64	0.60	0.99	0.40	1.08	0.58	0.65	0.61	39.85	38.68	39.02	0.00
Cl	0.16	0.19	0.18	0.19	0.17	0.16	0.25	–	–	0.17	0.20	0.19	0.37	0.37	0.38	0.00
Total	92.30	93.99	92.01	91.21	93.65	92.51	91.20	92.06	93.23	93.07	94.03	92.40	95.44	95.22	95.33	89.99

Note: Phase abbreviations: *Gl*, groundmass glass; *Apt*, apatite; and *Analc*, analcime. Dashes denote something that was not analyzed.

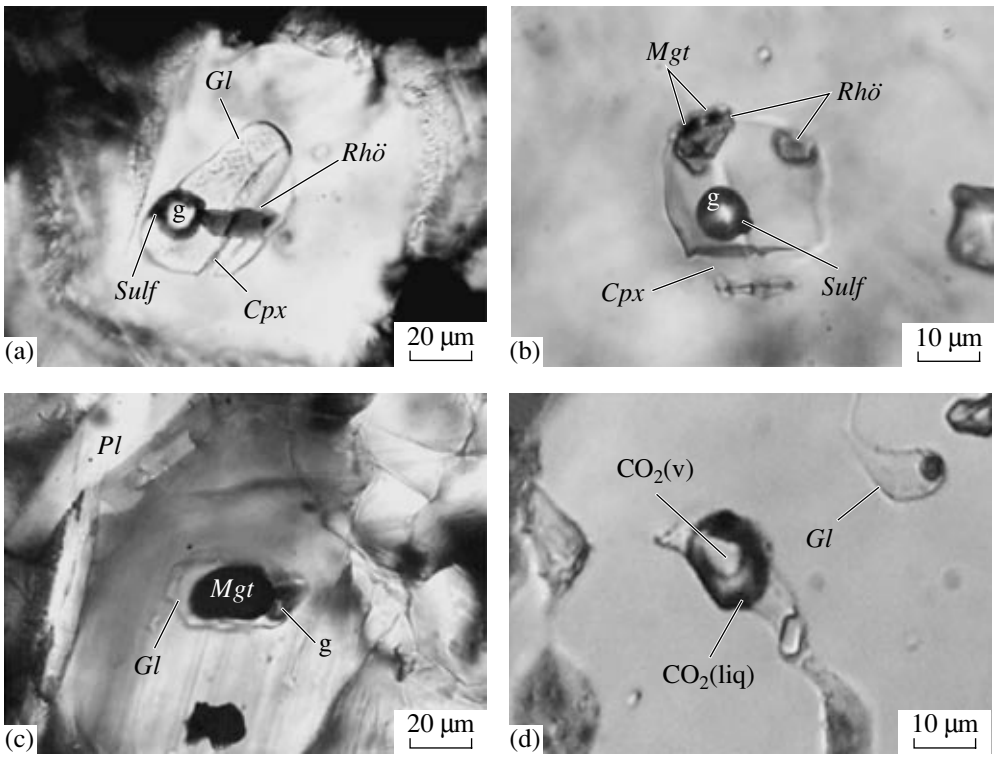

Fig. 4. Melt and fluid inclusions in minerals of the glassy basanites of the Tergesh pipe. (a) Primary melt inclusion in an olivine phenocryst. The inclusion is composed of glass + gas + rhönite + clinopyroxene + sulfide globule. Transmitted light. Sample Tsh-77. (b) Primary melt inclusion in an olivine phenocryst. Phase composition: glass + gas + rhönite + clinopyroxene + magnetite + sulfide globule. Transmitted light. Sample Tsh-77. (c) Primary melt inclusion in a zoned clinopyroxene phenocryst. Phase composition: glass + gas + xenogenous magnetite. Transmitted light. Sample Tsh-77. (d) Secondary fluid–melt and melt inclusions (glass + fluid + crystalline phases) in an olivine phenocryst. The fluid bubble is heterogeneous and consists of liquid and gaseous CO_2. $T = +18°C$. Transmitted light. Sample Tsh-78. Phase abbreviations: *Pl,* plagioclase; *Gl,* glass; g, gas; *Rhö*, rhönite; *Cpx,* clinopyroxene; *Mgt,* magnetite; *Sulf,* sulfide; CO_2(liq) liquid CO_2; and CO_2(v), CO_2 gas.

gate containing analcime, ilmenite, and apatite. This aggregate is a devitrification product after the groundmass glass of basanites.

Thus, the petrographic observations suggest the following sequence of the beginning of phase formation in the basanites: phenocrysts, olivine ⟶ clinopyroxene; groundmass, olivine ⟶ clinopyroxene, plagioclase, magnetite ⟶ apatite, ilmenite ⟶ glass and products of its devitrification.

MELT AND FLUID INCLUSIONS IN THE PHENOCRYSTS OF BASANITES

Inclusions in minerals were investigated in glassy basanite varieties. Melt and fluid inclusions were found only in olivine and clinopyroxene phenocrysts. Primary and secondary inclusions were distinguished in olivine.

Primary melt inclusions are confined mainly to the central parts of olivine grains and sometimes decorate growth zones of crystals. Their sizes range from 5 to 60 μm, and their shapes are rounded, oval, occasionally partly faceted. The inclusions consist of glass + low-density fluid ± daughter phases ± sulfide globule. The daughter phases are rhönite, clinopyroxene, occasionally apatite, Ti-magnetite, and ilmenite. Xenogenous Cr–Al spinel was sometimes observed. In some cases, the glass is finely crystallized. Relationships between the daughter phases in the inclusions suggest that rhönite was the earliest crystallizing phase followed by clinopyroxene and magnetite (ilmenite) (Figs. 4a, 4b).

During heating the first evidence for glass softening was observed at a temperature of <1000°C; ilmenite, clinopyroxene, and rhönite disappeared at 1030, 1150–1170, and 1230°C, respectively. The primary melt inclusions in olivine homogenized at 1280–1310°C. The inclusions that were heated without visual observation at temperatures of 1280–1320°C contained the following phases after quenching: glass + fluid ± sulfide globule. No high-density carbon dioxide phase was detected by the cryometric and Raman investigations of gas bubbles in the primary melt inclusions in olivine.

Secondary fluid and melt inclusions occur in groups and form trails along healed fractures. Such inclusions are sometimes interconnected. They have diverse shapes: rounded, oval, droplike, and irregular. The sizes of melt and fluid inclusions range within 5–40 and 3–30 μm, respectively. The phase composition of the secondary melt inclusions is glass + fluid ± ilmenite ± sul-

fide globule ± transparent crystals (presumably, clinopyroxene or apatite). The phase composition of the secondary fluid inclusions at $T = +18°C$ is liquid CO_2 + gaseous CO_2 (Fig. 4d).

The homogenization temperature of the secondary melt inclusions in olivine is 930–970°C. The characteristics of the cogenetic CO_2 inclusion (homogenization to a liquid phase at +24°C) indicate that the olivine phenocrysts crystallized and trapped the inclusions at $P > 3.5$ kbar.

The zoned clinopyroxene phenocrysts contain *primary melt inclusions* randomly distributed mainly in central zones and occasionally in marginal zones. The inclusions are from 5 to 55 μm in size and rounded, oval, droplike, and sometimes partly faceted in shape. Their phase composition is glass + low-density fluid ± xenogenous Ti-magnetite (Fig. 4c). The homogenization temperature of the primary melt inclusions in clinopyroxene is 1100°C.

CHEMICAL COMPOSITION OF INCLUSIONS

The heated inclusions in olivine show the following compositional variations (wt %): 41.2–46.5 SiO_2, 15.3–17.6 Al_2O_3, 2.2–3.2 TiO_2, 8.7–14.4 FeO, 3.2–8.6 MgO, 6.0–11.8 CaO, 0.8–1.2 P_2O_5, 4.1–5.8 Na_2O, and 1.9–3.0 K_2O. They are chemically very similar to the bulk composition of the basanites, except for they have lower alkali contents (Tables 1, 8; Fig. 5).

The residual glasses from the primary melt inclusions in olivine and clinopyroxene phenocrysts differ from the heated inclusions in olivine in higher contents of SiO_2 (49.5–57.3 wt %) and Al_2O_3 (21.0–27.5 wt %), and lower concentrations of TiO_2 (0.6–1.9 wt %) and other femic components (Tables 9, 10). Their compositions correspond to tephriphonolite and trachyandesite (Fig. 5). The concentration of CaO in the residual glasses varies considerably from 1.6 to 8.3 wt %, which is probably related to the amount of daughter Ca phases (clinopyroxene, rhönite, and apatite) that crystallized within the inclusions.

Clinopyroxene from the inclusions is significantly different from the clinopyroxene of phenocrysts and matrix of the basanites in SiO_2, Al_2O_3, and TiO_2 contents (Fig. 3). It is a Ti-augite (2.5–6.8 wt % TiO_2) with high Al_2O_3 (8.2–12.9 wt %) and P_2O_5 concentrations (0.2–1.3 wt %). It should be noted that high Al_2O_3 and P_2O_5 contents in daughter clinopyroxenes from melt inclusions in olivine were previously reported from the basanites of the Bele pipe (northern Minusinsk Depression) and trachybasalts of the southern Baikal volcanic area [11, 20].

Magnetite from the inclusions in olivine is enriched in TiO_2 (up to 23 wt %), and its composition approaches that of groundmass magnetite. Magnetite from inclusions in clinopyroxene is strongly different from the groundmass mineral in TiO_2, Cr_2O_3, and Al_2O_3 (Tables 5, 10).

The composition of rhönite is variable (wt %): 15.4–19.7 FeO, 29.4–24.7 SiO_2, 15.7–18.9 Al_2O_3, 8.9–11.4 TiO_2, and 0.02–1.4 Cr_2O_3 (Table 11). The presence of rhönite (mineral of the aenigmatite–rhönite group) in the inclusions in olivine of the basanites of the Tergesh pipe is intriguing, because this mineral was not found as a minor or accessory phase in the basanites. However, investigations during the past decades have demonstrated that this mineral is a widespread daughter phase in inclusions in olivine from many alkali basalts, and some alkali basalts contain rhönite as phenocrysts or in groundmass [21–29]. In the northern Minusinsk Depression, rhönite was previously reported as a daughter phase in some inclusions in olivine from the basanites of the Bele pipe [11]. However, it is more common as an interstitial phase in clinopyroxenite xenoliths from the basanites of the Bele, Krasnoozerskaya, and Botikha pipes [30]. The considerable chemical variability of the rhönite from melt inclusions in the Tergesh pipe suggests the importance of Na + Si $\longleftrightarrow$ Ca + Al substitution, whereas other substitution mechanisms are less distinct (Fig. 6). Based on the experimental data of Kunzmann et al. [21], Grapes et al. [31] proposed that the compositional variations of rhönite can be used as an indicator of oxygen fugacity variations. Given these relations, the compositions of rhönite from the Tergesh pipe suggest that during the crystallization of this mineral oxygen fugacity could vary from the NNO buffer to more reducing conditions of the IQF and QFM buffers (Fig. 6).

Unfortunately, the sulfide globules were too small (<5 μm) for microprobe analysis. The energy dispersive spectra of the sulfide globules indicate the presence of Fe and S and negligible amounts of Ni and Cu. Based on these observations, we supposed that the sulfide globules in the melt inclusions are dominated by pyrrhotite and contain minor amounts of chalcopyrite and pentlandite.

GEOCHEMICAL CHARACTERISTICS OF BASANITES

A comparison of the distribution of trace and rare earth elements in basalts from various geodynamic settings showed that the basanites of the Tergesh pipe are similar to ocean island basalts (OIB) [32] in light REE enrichment, positive Nb, and negative Pb anomalies (Fig. 7).

The abundances of major components in the basanites of the Tergesh pipe are also close to the average OIB composition, but the Tergesh basanites are characterized by elevated alkali and Al_2O_3 contents and low SiO_2 and MgO (Table 1).

The normalized multielement patterns (Fig. 7) of the basanites of the Tergesh pipe are generally similar to those of OIB, but are distinguished by higher contents

Table 8. Chemical compositions (wt %) of glasses from inclusions in olivine heated to temperatures of 1280–1320°C

T, °C	Phase composition*	Size, μm	*n*	SiO_2	TiO_2	Cr_2O_3	Al_2O_3	FeO	MnO	MgO	CaO	Na_2O	K_2O	P_2O_5	Cl	Total	*Fo**
1280°C	*Gl* + g	15	1	43.77	3.23	0.06	17.45	14.42	0.23	3.85	7.63	4.19	2.74	0.10	–	98.56	73
1280°C	*Gl* + *Sulf* + g	54	5	44.76	2.93	0.08	17.64	11.11	0.20	4.15	10.36	4.79	2.48	1.20	–	99.69	81
1280°C	*Gl* + *Sulf* + g	86	2	43.03	2.29	0.01	15.48	10.48	0.20	8.64	7.78	5.38	2.57	1.15	–	97.01	82
1280°C	*Gl* + g	37	2	43.42	3.24	0.02	16.99	12.59	0.22	5.01	9.26	4.68	2.71	1.04	–	99.18	78
1280°C	*Gl* + g	33	1	41.93	2.78	0.03	15.58	11.75	0.18	7.42	9.73	5.46	2.29	1.02	–	98.17	80
1280°C	*Gl* + g	18	1	41.91	3.08	0.05	16.17	12.00	0.15	6.37	9.10	5.15	2.44	1.10	–	97.52	80
1280°C	*Gl* + g	100	1	42.79	2.67	0.01	15.42	10.88	0.17	8.61	9.64	5.42	2.38	0.97	–	98.98	80
1300°C	*Gl* + g	33	2	41.92	2.69	0.18	15.64	12.05	–	4.99	11.83	5.37	1.98	0.91	0.04	97.58	80
1300°C	*Gl* + g	9	1	42.93	3.16	0.06	17.27	11.18	–	5.68	9.69	5.32	2.48	1.02	0.11	98.89	80
1300°C	*Gl* + g	14	2	42.13	2.83	0.05	15.76	12.27	–	6.67	10.58	5.03	2.22	1.01	0.09	98.64	80
1300°C	*Gl* + g	15	2	43.32	3.09	0.04	16.67	14.06	–	5.00	7.64	5.53	2.68	0.96	0.10	99.17	81
1300°C	*Gl* + g	9	2	42.50	3.33	0.05	17.44	12.71	–	6.27	6.80	5.05	2.76	1.15	0.09	98.15	79
1300°C	*Gl* + g	20	2	42.27	3.14	0.05	16.92	12.88	–	4.88	9.52	5.04	2.32	1.14	0.10	98.26	79
1300°C	*Gl* + g	13	1	43.34	3.00	0.03	17.37	12.67	–	3.28	8.94	5.37	2.58	1.13	0.11	97.82	79
1300°C	*Gl* + *Sulf* + g	37	1	45.37	2.22	0.02	17.39	8.73	–	6.35	6.95	5.83	3.03	1.17	0.10	97.16	84
1300°C	*Gl* + g	65	2	42.91	3.12	0.05	17.17	9.99	–	6.01	9.69	5.62	2.85	0.95	0.12	98.47	80
1300°C	*Gl* + g	14	1	43.14	2.93	0.03	16.04	10.91	–	8.18	8.70	5.42	2.64	0.97	0.10	99.06	80
1300°C	*Gl* + g	50	2	43.76	2.65	0.06	15.71	10.72	–	6.77	10.62	4.87	2.31	0.84	0.08	98.37	80
1300°C	*Gl* + g	45	2	42.14	3.01	0.04	15.59	12.87	–	7.63	9.47	4.92	2.33	0.82	0.10	98.91	78
1300°C	*Gl* + g	10	2	43.19	3.17	0.04	17.52	11.60	–	7.83	6.05	4.48	2.82	0.96	0.08	97.71	79
1320°C	*Gl* + g	72	2	43.98	2.83	0.08	15.84	12.39	0.19	5.71	9.95	4.52	2.18	0.98	–	98.63	81
1320°C	*Gl* + g	22	2	42.55	3.11	0.08	16.94	14.17	0.23	4.74	7.99	5.28	2.42	1.04	–	98.55	77
1320°C	*Gl* + g	15	2	43.73	3.00	0.02	15.92	14.28	0.34	3.94	9.49	4.34	2.35	0.92	–	98.32	78
1320°C	*Gl* + g	37	2	46.55	2.77	0.08	16.73	11.54	0.20	5.17	8.00	4.49	2.74	1.04	–	99.31	82
1320°C	*Gl* + *Sulf* + g	25	1	41.23	3.07	0.03	15.71	13.91	0.28	4.05	9.30	5.24	2.40	1.18	–	96.40	73
1320°C	*Gl* + g	23	1	41.53	2.88	0.09	15.33	13.15	0.26	5.47	9.84	4.91	2.37	1.07	–	96.89	76
1320°C	*Gl* + *Sulf* + g	31	1	42.45	2.87	0.05	15.60	14.24	0.25	5.49	9.11	5.18	2.29	0.94	–	98.47	76

Note: Phase abbreviations: *Gl*, glass; *Sulf*, sulfide; and g, gas. *n* is the number of analyses. Dashes denote something that was not analyzed. *Fo** is the composition of the host mineral.
*Phase composition of heated inclusion.

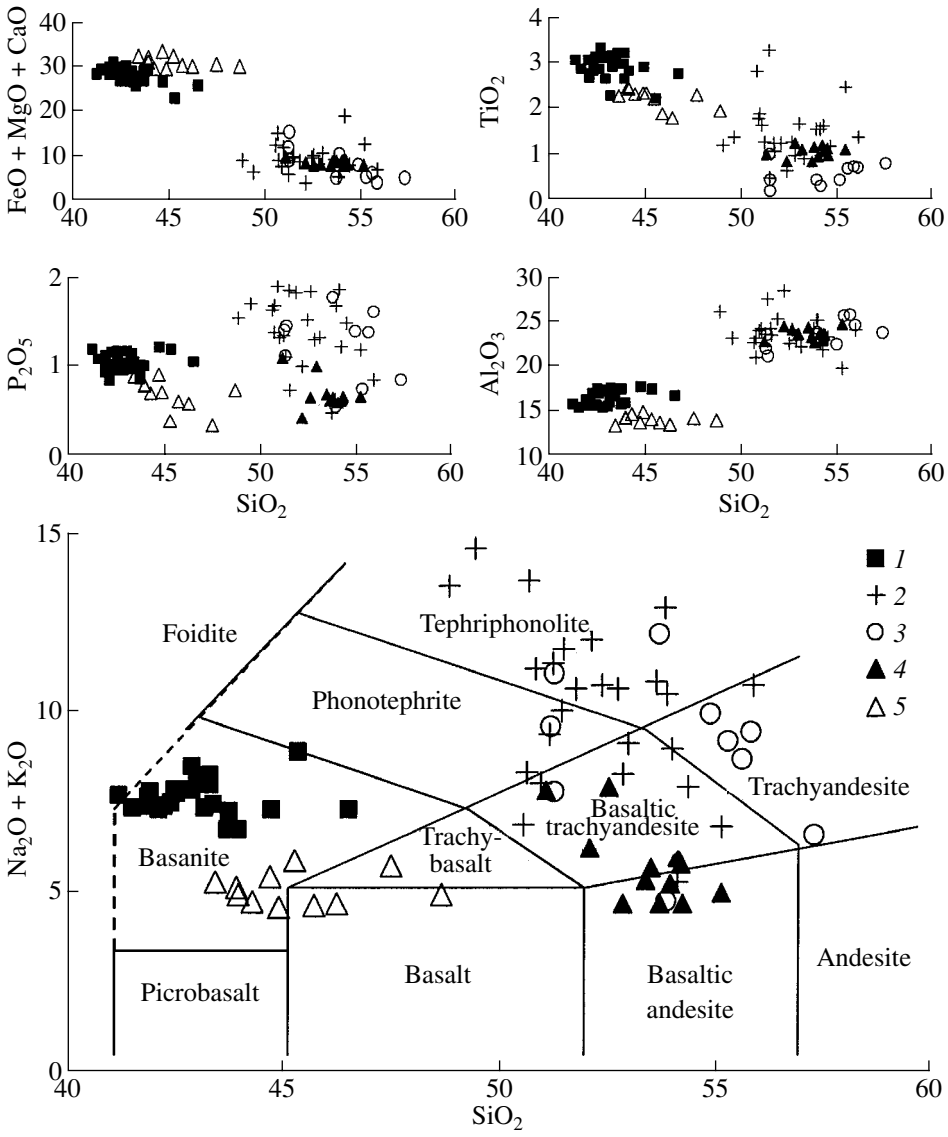

Fig. 5. Variations in the composition of glasses from inclusions in minerals of the glassy basanites of the Tergesh pipe. (*1*) Glasses from heated inclusions in olivine, (*2*) residual glasses from inclusions in olivine, (*3*) residual glasses from inclusions in clinopyroxene, (*4*) groundmass glass of basanites, and (*5*) basanite (after [2, 7–9] and our data). The ($Na_2O + K_2O$)–SiO_2 classification diagram is after [19].

of Ba, Th, U, Ta, Nb, La, Ce, Pb, Nd, and Sr and lower contents of Rb, Hf, Zr, Sm, Eu, Ti, and heavy REE. The low concentration of Rb is primarily related to its mobile behavior and the absence of potassium-rich phases. Of particular interest is the enrichment in light REE: the La/Lu ratio is 255–262, which is much higher than the average value of OIB-type sources (La/Lu = 123). Since the basanites are slightly depleted in heavy REE, it can be supposed that they were derived from a garnet-bearing source. It is worth noting that the basanites of the Tergesh pipe contain garnet-bearing mantle xenoliths [10]. The enrichment of lithophile elements in the groundmass glass (which can be considered as a derivative of the initial melt) is probably related to crystal fractionation. The model age of basanite relative to the depleted mantle (DM) is 427–446 Ma. The present-day ε_{Nd} value is +5.5, which suggests that the basanites were derived from a depleted source.

The $^{143}Nd/^{144}Nd$ ratios of the basanites range from 0.512876 to 0.512891, and $^{87}Sr/^{86}Sr$, from 0.70346 to 0.70366 [33]. Their compositions plot in the Sr–Nd isotopic diagram near the mixing line between primitive and depleted mantle sources (Fig. 8). There was also a contribution from a HIMU-type source (recycled oceanic crust), which is also suggested by the elevated Nb/U ratio (56) compared with the primitive mantle value of Nb/U = 30.

Table 9. Chemical compositions (wt %) of residual glasses and daughter phases from unheated inclusions in olivine

Phase composition of inclusion	Size, μm	*n*	Phase	SiO_2	TiO_2	Cr_2O_3	Al_2O_3	FeO	MnO	MgO	CaO	BaO	Na_2O	K_2O	P_2O_5	Cl	Total
Gl + *Cpx* + *Rhö* + g	30	1	*Gl*	53.92	1.00	0.00	25.17	2.09	0.03	0.43	3.49	0.15	5.02	5.44	1.67	0.32	98.73
		1	*Cpx*	43.65	4.04	0.03	9.43	7.17	0.14	11.11	22.34	0.00	0.67	0.00	1.26	0.00	99.84
		2	*Rhö*	28.07	10.22	0.19	16.53	17.01	0.14	13.26	11.30	0.00	1.58	0.00	0.00	0.00	98.29
Gl + *Cpx* + g	63	1	*Gl*	48.83	1.21	0.00	26.17	4.25	0.04	0.41	3.59	–	9.57	3.91	1.53	–	99.51
		1	*Cpx*	40.26	5.63	0.05	11.07	8.64	0.08	9.99	21.87	–	0.70	0.00	0.43	–	99.34
Gl + *Cpx* + *Rhö* + g	44	1	*Cpx*	44.51	4.13	0.12	9.31	7.90	0.11	13.05	19.24	0.00	0.80	0.00	0.76	0.00	99.92
		1	*Rhö*	26.31	9.68	0.99	17.21	19.74	0.08	13.29	11.27	0.00	1.14	0.00	0.00	0.00	99.71
Gl + *Cpx* + g	20	1	*Gl*	51.82	1.25	0.00	25.32	2.54	0.04	0.87	4.60	0.04	7.89	2.73	1.82	0.14	99.06
		1	*Cpx*	42.34	5.67	0.02	11.88	7.30	0.11	9.35	21.16	0.00	0.89	0.00	0.61	0.00	99.32
Gl + *Cpx* + g	48	1	*Gl*	50.86	1.65	0.04	24.03	2.83	0.07	0.51	3.52	0.24	4.52	6.66	1.90	0.22	97.05
		1	*Cpx*	43.24	5.34	0.15	10.39	5.81	0.16	11.50	22.35	0.00	0.69	0.00	0.08	0.00	99.66
Gl + *Cpx* + *Rhö* + g	40	1	*Gl*	52.79	1.68	0.00	22.99	3.90	0.07	0.17	3.46	–	5.26	5.35	1.29	–	96.95
		1	*Rhö*	24.89	10.54	0.92	17.02	19.73	0.14	12.37	11.49	–	0.94	0.00	0.00	–	98.04
		1	*Cpx*	41.61	5.99	0.00	11.41	7.15	0.11	9.76	21.91	–	0.71	0.00	1.16	–	99.81
Gl + *Cpx* + g	16	1	*Gl*	52.16	0.66	0.00	28.52	1.38	0.01	0.19	1.89	0.00	9.55	2.44	0.99	0.02	97.80
		1	*Cpx*	43.47	4.72	0.31	10.88	6.08	0.09	10.80	21.38	0.00	1.54	0.00	0.28	0.00	99.56
Gl + *Cpx* + *Rhö* + g	20	1	*Gl*	51.26	0.51	0.00	27.58	1.69	0.01	1.38	2.07	0.00	9.58	1.73	1.09	0.03	96.93
		1	*Cpx*	42.60	2.54	0.02	8.19	8.62	0.01	15.16	20.03	0.00	0.69	0.00	0.63	0.00	98.57
		1	*Rhö*	29.40	9.23	0.58	16.16	15.42	0.13	13.82	12.99	0.00	1.13	0.00	0.00	0.00	98.85
Gl + *Cpx* + *Rhö* + *Sulf* + g	52	1	*Gl*	53.87	1.56	0.00	25.15	2.62	0.05	0.39	1.64	0.20	6.73	6.14	0.62	0.24	99.20
		1	*Rhö*	25.07	10.87	0.15	17.62	19.30	0.14	13.19	10.77	0.00	1.52	0.00	0.00	0.00	98.62
Gl + *Sp* + *Rhö* + *Sulf* + g	26	1	*Gl*	52.57	1.00	0.00	24.08	2.30	0.07	2.58	4.36	0.11	3.63	4.11	1.84	0.21	96.86
		1	*Rhö*	26.56	8.90	3.27	18.15	15.56	0.11	13.50	11.49	0.00	1.11	0.00	0.00	0.00	98.64
		1	*Sp*	–	1.93	20.01	35.58	26.65	0.20	13.42	–	–	–	–	–	–	97.79
Gl + *Cpx* + *Rhö* + g	22	2	*Gl*	49.44	1.38	0.00	23.23	3.19	0.68	0.55	1.98	–	5.96	8.59	1.70	–	96.09
		1	*Cpx*	41.83	4.64	0.23	9.53	6.65	0.11	12.51	22.03	–	0.74	0.00	0.00	–	98.28
		1	*Rhö*	24.91	9.88	0.98	15.56	19.73	0.16	13.72	10.99	–	1.66	0.00	0.00	–	97.59
Gl + *Cpx* + g	36	1	*Gl*	50.72	1.89	0.00	23.19	3.76	0.05	0.63	3.97	–	6.11	7.52	1.68	–	99.52
Gl + *Rhö* + *Mgt* + g	43	2	*Gl*	53.67	1.55	0.01	24.23	3.10	0.07	0.60	4.80	0.14	6.91	3.90	0.47	0.15	99.58

Note: Phase abbreviations: *Gl*, glass; *Rhö*, rhönite; *Sp*, spinel; *Cpx*, clinopyroxene; *Sulf*, sulfide; *Mgt*, magnetite; and g, gas. *n* is the number of analyses, and dashes denote something that was not analyzed.

Table 10. Chemical compositions (wt %) of residual glasses and daughter phases from unheated inclusions in clinopyroxene

Phase composition of inclusion	Size, μm	Phase	*n*	SiO_2	TiO_2	Cr_2O_3	V_2O_3	Al_2O_3	FeO	MnO	MgO	CaO	BaO	SrO	Na_2O	K_2O	P_2O_5	Cl	Total
Gl + *Mgt*	26	*Gl*	1	53.91	0.32	0.36	–	23.82	4.74	0.09	3.29	1.47	0.03	–	4.07	0.61	0.54	0.02	93.27
		Mgt	1	0.46	16.61	2.00	–	8.33	63.79	0.54	4.55	0.27	–	–	–	0.00	0.00	0.00	96.55
Gl + g	16	*Gl*	1	51.32	0.22	0.00	–	21.12	5.91	0.20	2.17	6.47	0.16	0.12	4.44	3.32	1.44	0.16	97.05
Gl + g	23	*Gl*	1	53.74	0.47	0.03	–	23.00	2.14	0.13	0.65	1.68	0.15	0.12	7.41	4.73	1.77	0.21	96.23
Gl + *Mgt* + g	31	*Mgt*	1	0.30	14.19	1.45	–	8.54	63.97	0.51	6.64	0.25	–	–	–	0.00	0.00	0.00	95.85
Gl + g	34	*Gl*	1	55.64	0.75	0.00	–	25.82	2.69	0.12	0.75	1.99	0.18	0.15	4.00	4.65	1.37	0.24	98.34
Gl + *Mgt* + g	38	*Mgt*	1	0.14	15.49	0.72	–	7.92	64.27	0.41	6.77	0.31	–	–	–	0.00	0.00	0.00	96.03
Gl + *Mgt* + g	51	*Gl*	1	57.34	0.80	0.00	–	23.78	1.87	0.02	0.84	1.60	0.05	–	3.43	3.11	0.84	0.19	93.87
		Mgt	1	0.13	15.01	0.91	–	8.51	64.45	0.57	6.59	0.39	–	–	–	0.00	0.00	0.00	96.56
Gl + *Mgt* + g	17	*Gl*	1	55.32	0.71	0.01	–	25.67	2.99	0.08	0.43	1.28	0.14	–	4.53	4.62	0.73	0.17	96.68
Gl + *Mgt* + g	35	*Gl*	2	55.88	0.73	0.02	–	24.66	1.69	0.08	0.50	1.08	0.13	0.15	4.68	4.73	1.61	0.17	96.10
		Mgt	1	–	11.38	0.44	0.31	10.35	67.14	0.62	5.34	–	–	–	–	–	–	–	95.58
Gl + g	9	*Gl*	1	51.3	0.46	0.00	–	23.56	4.57	0.10	1.31	2.34	0.12	0.01	6.55	4.49	1.10	0.12	96.03
Gl + *Mgt* + g	18	*Gl*	1	51.25	1.02	0.02	–	21.98	3.35	0.13	1.72	6.09	0.17	0.09	5.94	3.63	1.39	0.12	96.90
Gl + *Mgt* + g	28	*Gl*	1	54.92	0.46	0.15	–	22.41	4.38	0.11	0.86	2.08	0.13	0.10	5.38	4.52	1.38	0.20	97.07

Note: Phase abbreviations: *Gl*, glass; *Mgt*, magnetite; and g, gas. *n* is the number of analyses, and dashes denote something that was not analyzed.

Table 11. Chemical compositions (wt %) of rhönite from inclusions in olivine

Component	1	2	3	4	5	6	7	8	9	10	11	12	13	14	15	16	17
SiO_2	28.25	26.53	26.31	26.95	28.07	29.40	25.22	25.44	25.07	25.53	26.56	24.77	26.52	26.27	24.91	24.79	24.89
TiO_2	10.37	9.91	9.68	9.93	10.22	9.23	10.47	10.46	10.87	10.05	8.90	9.53	9.81	11.38	9.88	10.09	10.54
Cr_2O_3	0.27	1.00	0.99	1.41	0.19	0.58	0.49	1.13	0.15	0.31	3.27	0.31	0.34	0.02	0.98	1.09	0.92
Al_2O_3	17.16	18.85	17.21	17.13	16.53	16.16	17.03	18.20	17.62	17.19	18.15	17.68	16.91	15.70	15.56	17.10	17.02
FeO	18.52	18.38	19.74	17.56	17.01	15.42	17.96	16.67	19.30	19.32	15.56	19.61	17.90	19.58	19.73	19.74	19.73
MnO	0.13	0.14	0.08	0.12	0.14	0.13	0.13	0.10	0.14	0.11	0.11	0.13	0.12	0.12	0.16	0.16	0.14
MgO	12.32	12.06	13.29	13.34	13.26	13.82	14.09	13.31	13.19	12.79	13.50	13.69	13.70	13.99	13.72	12.69	12.37
CaO	10.68	10.22	11.27	11.23	11.30	12.99	11.31	11.59	10.77	11.29	11.49	11.13	11.47	11.36	10.99	11.74	11.49
Na_2O	1.77	1.48	1.14	1.49	1.58	1.13	1.37	1.20	1.52	1.08	1.11	1.35	1.22	1.28	1.66	0.99	0.94
Total	99.48	98.57	99.71	99.16	98.29	98.85	98.07	98.09	98.62	97.67	98.64	98.21	97.99	99.70	97.59	98.40	98.04
Fe_2O_3	1.57	1.70	5.65	4.01	2.17	0.64	7.37	3.61	6.88	5.03	2.11	9.59	4.95	6.10	10.86	6.42	4.66
FeO	17.11	16.85	14.66	13.95	15.05	14.84	11.33	13.42	13.11	14.79	13.66	10.98	13.45	14.09	9.96	13.96	15.54
Total	99.63	98.74	100.28	99.56	98.50	98.92	98.81	98.45	99.31	98.17	98.85	99.17	98.49	100.31	98.67	99.04	98.51

Note: FeO and Fe_2O_3 were calculated assuming ideal stoichiometry.

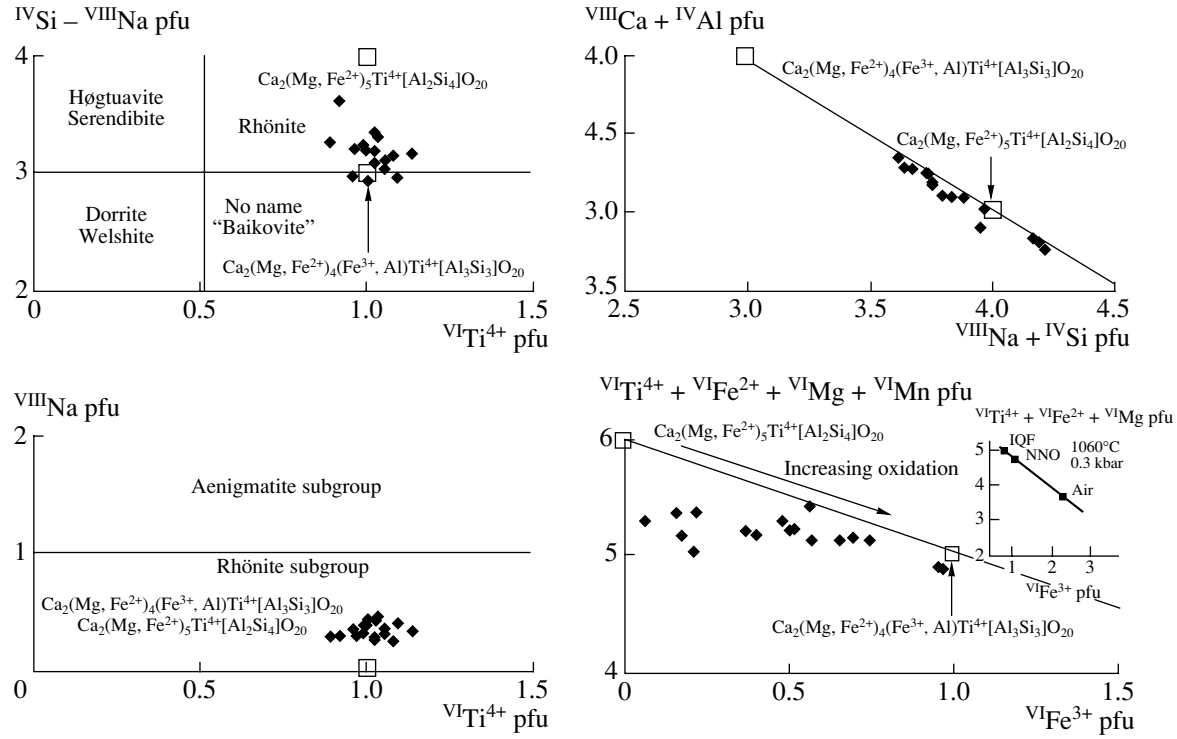

Fig. 6. Variations in the composition of rhönite from melt inclusions in olivine of the Tergesh pipe. The classification diagrams Si–Na–Ti and Na–Ti are after [23]; Ca + Al versus Na + Si and Ti + Fe^{2+} + Mg + Mn versus Fe^{3+} are after [31]. The inset in the lower right panel is after [21].

DISCUSSION

Evolution of Basanite Melt during Crystallization

The investigation of the composition of heated and residual glasses in inclusions in minerals provides insight into the liquid line of descent of the initial melt. The main assumption is that the composition of glass from inclusions heated to homogenization temperatures is sufficiently close to the composition of the melt at the moment of its entrapment by the host mineral, and the residual glasses of unheated inclusions are its derivatives.

Figure 5 shows variations in the compositions of glasses from inclusions (heated and residual) compared with the basanite of the Tergesh pipe (as a possible primary melt) and groundmass glass (derivative of the primary melt). It can be seen that the basanite melt evolved during crystallization along a miaskitic trend toward an increase in SiO_2, Al_2O_3, and alkalis and a decrease in femic components. The same character of basanite melt evolution was previously established for the Bele pipe, which is the southernmost pipe of the northern Minusinsk Depression [11]. It should be noted that such a melt evolution is typical of alkaline rocks of the miaskitic series from various regions of the world [36–39 and many others].

According to petrographic observations, the possible sequence of the onset of phase crystallization in the glassy basanites is the following: phenocrysts, olivine ⟶ cli-

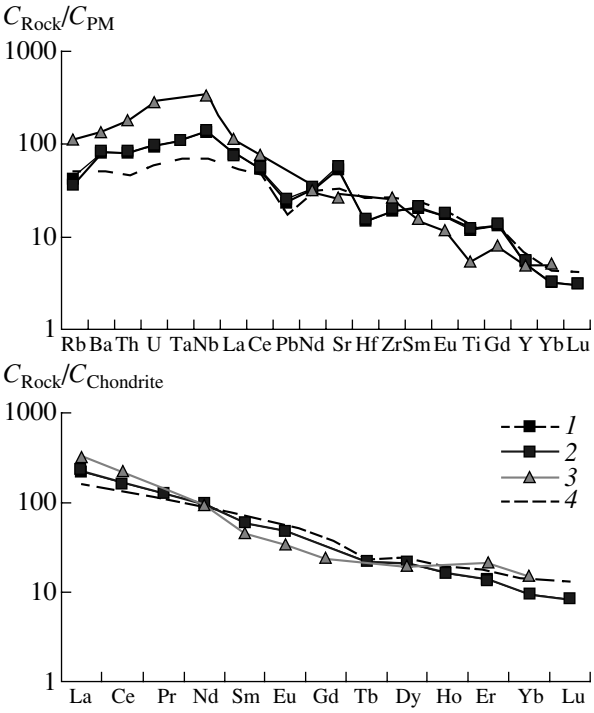

Fig. 7. Distribution of trace and rare earth elements in the basanites of the Tergesh pipe. (*1*) and (*2*) basanites [33]; (*3*) groundmass glass of basanites (our data); and (*4*) average composition of OIB [34]. The concentrations of trace elements are normalized to primitive mantle (PM) values, and rare earth elements, to chondrite values after [34].

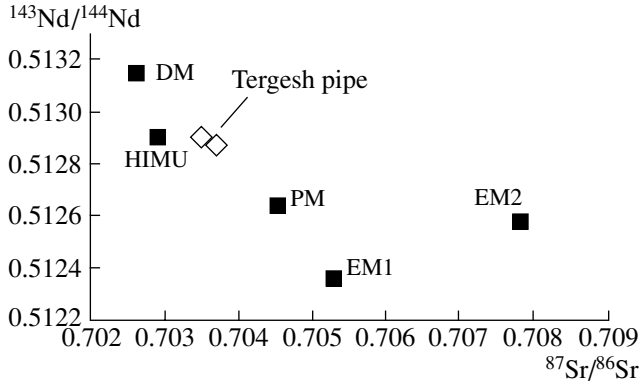

Fig. 8. Relationships of $^{87}Sr/^{86}Sr$ and $^{143}Nd/^{144}Nd$ in the basanites of the Tergesh pipe. Model mantle components are given after [35]: PM, primitive mantle; DM, depleted mantle; EM1 and EM2, enriched mantle reservoirs; and HIMU, enriched high-U/Pb material. The data for the basalts of the Tergesh pipe are taken from [33].

nopyroxene; groundmass, olivine ⟶ clinopyroxene, plagioclase, magnetite ⟶ apatite, ilmenite ⟶ glass. The relationships of daughter phases and thermometric experiments suggest the following sequence of crystallization in the melt inclusions: rhönite ⟶ clinopyroxene, magnetite (ilmenite) ⟶ glass.

The analyses of heated glasses (Table 8) show the predominance of sodium over potassium, but the general melt evolution suggests a gradual accumulation of potassium. Glass is the only potassium-rich phase in the glassy basanites. Potassium feldspar and occasionally biotite and nepheline were formed during the late stages of crystallization in the holocrystalline rocks of the Tergesh pipe and other pipes of the northern Minusinsk Depression [11].

In general, the alkaline magmatism of the Minusinsk Depression and adjacent areas has always showed a distinct sodic character, from the Paleozoic to the Cenozoic. The diatremes are spatially associated with the large alkaline massif Kiya-Shaltyr', other alkaline intrusions, and numerous dikes and bodies of nephelinites and other rocks of Paleozoic and younger ages [1, 40].

An important problem for the basanites of the Minusinsk Depression is the content of water in the initial melt and its derivatives. Unfortunately, the small sizes of melt inclusions prevented an ion microprobe analysis for the determination of water content. The relatively high totals of oxides in the electron microprobe analyses of heated and residual glasses from primary inclusions and the absence of hydrous phases indicate that the initial basanite melt of the Tergesh pipe was relatively poor in water. In principle, water could be accumulated during the evolution of the basanite melt. The groundmass glass shows relatively low alkali concentrations and is water-saturated (up to 6 wt % H_2O). In our opinion, the high contents of water in the glass of the basanite matrix are probably related to postmagmatic processes. Glass could be enriched in water and simultaneously depleted in alkalis during cooling. These processes were most likely responsible for the appearance of analcime in the basanites of the Tergesh pipe. Its formation can be attributed to two factors: (1) high concentrations of sodium in the residual basanite melt (groundmass glass) and (2) devitrification of this glass owing to either autometasomatism or under the influence of water from the sedimentary country rocks.

P–T–f_{O_2} Conditions of Basanite Melt Crystallization

The depths of melt generation and crystallization conditions are the main problems for the basanites of the Tergesh pipe. Unfortunately, very little data is available on the source and depth of generation of the initial basanite melt. The geochemistry of rocks suggests their mantle source. The presence of garnet-bearing mantle xenoliths in the basanites of the Tergesh pipe indirectly indicates that this source occurred at depths of more than 60 km [15]. It is commonly accepted that primary basaltic melts from peridotite must contain at least 200 ppm Ni and 500 ppm Cr and 10–14% MgO. With respect to these parameters, the basanites of the Tergesh pipe can be considered as approaching the compositions of primary mantle melts affected by crystallization differentiation. The isotope geochemical investigation of clinopyroxenes and basanites from the Tergesh, Kongarovskaya, and Krasnoozerskaya pipes suggested that the carbonatite metasomatism of upper mantle rocks was nearly synchronous with the formation of basanite melts [10].

The presence of CO_2 inclusions in olivine phenocrysts from the basanites of the Tergesh pipe suggests that the phenocrysts began crystallizing at a pressure of 3.5 kbar, and the groundmass minerals crystallized under near surface conditions. According to thermometric experiments, the olivine crystallized at 1280–1320°C.

The presence of rhönite in the melt inclusions in olivine from the basanites of the Tergesh pipe seems to provide some insight into the pressure of crystallization in the inclusions in olivine. However, pressure estimates for rhönite are still controversial. This problem was considered in detail by Sharygin et al. [29]. On the one hand, according to the data of Kunzmann [22, 23], rhönite is stable in alkali basalts within a temperature interval of 840–1200°C and pressures of less than 0.6 kbar. On the other hand, it may be stable in deep-seated xenoliths up to 5 kbar [21]. The data reported here and the results of our previous investigation of melt inclusions [29] suggest that rhönite can be stable at temperatures of more than 1200°C and at pressures from 5–6 kbar to one atmosphere.

The coexistence of olivine and Cr spinel, the chemical composition of rhönite, and the mineralogy of basanites allow us to estimate oxygen fugacity during

various stages of basanite melt crystallization in the Tergesh pipe. The earliest olivine–spinel pairs crystallized at an oxygen fugacity corresponding approximately to the NNO buffer [17, 18]. Later stages occurred under progressively more reducing conditions (near the QFM buffer). This is suggested by the chemistry of rhönite, the significant fraction of ulvospinel in magnetite, and the appearance of ilmenite.

CONCLUSIONS

The following conclusions were drawn from the data obtained for the basanites of the Tergesh pipe.

(1) The following crystallization sequence was established for the basanites: phenocrysts, olivine ($T >$ 1300°C) ⟶ clinopyroxene ($T >$ 1100°C); groundmass, olivine ⟶ clinopyroxene, plagioclase, magnetite ⟶ apatite, ilmenite ⟶ glass. The phases of melt inclusions in olivine phenocrysts appeared in the following sequence: rhönite ($T \le$ 1230°C) ⟶ clinopyroxene (1150–1170°C) ⟶ ilmenite, magnetite ($T \le$ 1030°C) ⟶ glass ($T \le$ 1000°C). The crystallization of olivine phenocrysts began at $P >$ 3.5 kbar, whereas groundmass minerals were formed under near surface conditions. Oxygen fugacity gradually changed during the crystallization of basanites from oxidized (NNO) to more reduced conditions (QFM).

(2) The general trend of melt evolution during basanite crystallization included an increase in SiO_2, Al_2O_3, and alkali contents and a decrease in femic components, and the composition changed from basanite to tephriphonolite and trachyandesite.

(3) Given the enrichment in compatible trace elements (65–170 ppm Ni and 140–515 ppm Cr) and the high MgO content (8.1–10.7 wt %), it can be supposed that the composition of basanites from the Tergesh pipe approaches primary mantle melts affected by differentiation.

ACKNOWLEDGMENTS

The authors thank L.N. Pospelova (Joint Institute of Geology, Geophysics, and Mineralogy, Siberian Division, Russian Academy of Sciences) for help with microprobe analysis; N.V. Maksimova (Joint Institute of Geology, Geophysics, and Mineralogy, Siberian Division, Russian Academy of Sciences) for the SR XRF data on the basanites of the Tergesh pipe; S.V. Kovyazin and E.I. Petrushin (Institute of Mineralogy and Petrography, Siberian Division, Russian Academy of Sciences) for thermometric experiments; S. Simakin and E. Potapov (Institute of Microelectronics, Russian Academy of Sciences, Yaroslavl) for the ion probe analysis of glass. We also grateful to V.G. Mal'kovets (Institute of Mineralogy and Petrography, Siberian Division, Russian Academy of Sciences) and Yu.D. Litasov (Institute of Geology, Siberian Division, Russian Academy of Sciences), who provided their data on the isotopic systematics and ICP MS analyses of the rocks of the Tergesh pipe, and also to V.B. Naumov (Institute of Geochemistry and Analytical Chemistry, RAS, Moscow) for constructive remarks of this article. This study was financially supported by the Russian Foundation for Basic Research (project nos. 02-05-64620, 03-05-64030, and 04-05-64358) and the Ministry of Industry and Science of the Russian Federation (grant no. NSh-93.2003.50).

REFERENCES

1. I. V. Luchitskii, *Volcanism and Tectonics of the Devonian Depressions of the Minusinsk Basin* (Akad. Nauk SSSR, Moscow, 1960) [in Russian].
2. A. V. Kryukov and Z. V. Kryukova, "Pyropes from the Tergesh Pipe," in *Materials on the Geology and Mineral Resources of the Krasnoyarsk Region* (Krasnoyarsk, 1962), no. 3, pp. 131–140 [in Russian].
3. A. V. Kryukov, "New Type of Explosion Pipes in the Southwestern Framing of the Siberian Craton," in *Geology of the Southwestern Framing of the Siberian Craton* (Nedra, Moscow, 1964), pp. 196–240 [in Russian].
4. A. V. Kryukov, "Main Features of the Diamond Potential of the Krasnoyarsk Region," in *Materials on the Metallogeny and Mineral Resources of the Krasnoyarsk Region* (Krasnoyarsk, 1968), pp. 155–171 [in Russian].
5. V. A. Kutolin and V. M. Frolova, "Petrology of Ultrabasic Nodules in Basalts of the Minusinsk Depression and Transbaikalia and Composition of the Earth's Upper Mantle," in *Problems of the Petrology of Basic and Ultrabasic Rocks* (Nauka, Moscow, 1972), pp. 55–59 [in Russian].
6. B. M. Vladimirov, N. Ya. Volyanyuk, and A. I. Ponamorenko, *Deep-Seated Inclusions from Kimberlites, Basalts, and Kimberlite-Like Rocks* (Nauka, Moscow, 1976) [in Russian].
7. V. P. Kostyuk, E. A. Kostyuk, T. Yu. Bazarova, et al., "Minerals and Origin of Deep-Seated Inclusions in the Basalts of the Minusinsk Depression," in *Materials on Genetic Mineralogy and Petrology* (Novosibirsk, 1977), pp. 175–191 [in Russian].
8. N. V. Sobolev, V. V. Kepezhinskas, Yu. I. Ovchinnikov, and N. P. Pokhilenko, *Mantle Xenoliths in Meso–Cenozoic Volcanic Pipes of Khakassia* (IGiG SO AN SSSR, Novosibirsk, 1988) [in Russian].
9. I. V. Ashchepkov, V. V. Kepezhinskas, V. G. Malkovets, and Yu. I. Ovchinnikov, *Mantle Xenoliths from the Meso-Cenozoic Volcanic Pipes of Khakassia* (UIGGM SD RAS, Novosibirsk, 1995) [in Russian].
10. V. G. Malkovets, Candidate's Dissertation in Geology and Mineralogy (Novosibirsk, 2001).
11. A. V. Golovin, V. V. Sharygin, and V. G. Malkovets, "Evolution of Melt during the Crystallization of Basanites of the Bele Pipe (Northern Minusinsk Depression)," Geol. Geofiz. **41**, 1760–1782 (2000).
12. V. S. Zubkov, V. N. Smirnov, G. S. Plyusnin, et al., "First K–Ar Datings and Strontium Isotope Systematics of the Basanite Pipes of the Chulym–Yenisei Depression," Dokl. Akad. Nauk SSSR **307**, 1466–1469 (1989).

13. V. Yu. Bragin, V. N. Reutskii, K. D. Litasov, and V. G. Malkovets, "Late Cretaceous Episode of within-Plate Magmatism in the Northern Minusinsk Depression: Evidence from Paleomagnetic and Geochronological Data," Geol. Geofiz. **40**, 576–582 (1999).
14. V. G. Malkovets, A. V. Travin, Yu. D. Litasov, et al., "Volcanic Pipes as Clues to Upper Mantle Petrogenesis: Mesozoic Ar–Ar Dating of the Minusinsk Basalts, South Siberia," Inter. Geol. Review **45** (2), 133–142 (2003).
15. V. G. Malkovets, D. A. Ionov, W. L. Griffin, et al., "A P–T Composition Cross-Section of Spinel and Garnet Facies Lithospheric Mantle in the Minusa Region, SW of the Siberian Craton," in *Proceedings of 7th International Kimberlite Congress, Cape Town, South Africa, 1998* (Cape Town, 1998), pp. 543–545.
16. E. I. Petrushin, L. Sh. Bazarov, E. I. Gordeeva, and V. V. Sharygin, "Thermometric Stage for Petrological Investigations of Alkaline Igneous Rocks," Prib. Tekh. Eksp. **46** (2), 108–112 (2003).
17. J. Fabries, "Spinel–Olivine Geothermometry in Peridotites from Ultramafic Complexes," Contrib. Mineral. Petrol. **69**, 329–336 (1979).
18. C. Ballhaus, R. F. Berry, and D. H. Green, "High Pressure Experimental Calibration of the Olivine–Orthopyroxene–Spinel Oxygen Geobarometer: Implications for the Oxidation State of the Upper Mantle," Contrib. Mineral. Petrol. **107**, 27–40 (1991).
19. V. E. Sklyarov, *Interpretation of Geochemical Data* (Intermet Inzhiniring, Moscow, 2001) [in Russian].
20. V. B. Naumov, M. V. Portnyagin, M. L. Tolstykh, and V. V. Yarmolyuk, "Composition of Magmatic Melts from the Southern Baikal Volcanic Region: A Study of Inclusions in Olivine from Trachybasalts," Geokhimiya, No. 3, 243–253 (2003) [Geochem. Int. **41**, 213–223 (2003)].
21. Th. Kunzmann, G. Spicker, and H. G. Huckenholz, "Stabilitat von Rhonit in naturlichen und synthetischen Paragenesen," Fortsch. Mineral. **64** (1), 92 (1986).
22. Th. Kunzmann, Ph. Dissertation (Universitat Munchen, Munchen, 1989).
23. Th. Kunzmann, "The Aenigmatite–Rhonite Mineral Group," Eur. J. Mineral. **11**, 743–756 (1999).
24. M. C. Magonthier and D. Velde, "Mineralogy and Petrology of Some Tertiary Leucite–Rhonite Basanites from Central France," Mineral. Mag. **40**, 817–826 (1976).
25. H. B. Olsson, "Rhonite from Skane (Scania), Southern Sweden," Geol. Fören. Stockholm Förh. **105**, 281–286 (1983).
26. I. Seghedi, O. Vaselli, and H. Downes, "Occurrence of Rhonite in Basanites from Poiana Rusca Mountains, Romania," Rom. J. Mineral. **77**, 41 (1995).
27. T. Prestvik, T. Torske, B. Sundvoll, and H. Karlsson, "Petrology of Early Tertiary Nephelinites off Mid-Norway. Additional Evidence for an Enriched Endmember of the Ancestral Iceland Plume," Lithos **46**, 317–330 (1999).
28. D. V. Kuz'min, V. P. Chupin, and B. A. Litvinovskii, "Temperature and Composition of Magmas of the Trachybasalt–Comendite Rock Associations of the Tsagan–Khurtei Range, Western Transbaikalia: Evidence from Mineral Inclusions," Geol. Geofiz. **40** (1), 62–72 (1999).
29. V. V. Sharygin, K. Kóthay, M. Petö, et al., "Rhönite in Alkali Basalts: Studies of Silicate Melt Inclusions in Olivine Phenocrysts," Acta Mineral. Petrogr., Abstr. Ser. Szeged **2**, 182–183 (2003).
30. A. V. Golovin, V. V. Sharygin, and V. G. Malkovets, "Interstitial Associations in Deep-Seated Xenoliths from the Pipes of the Northern Minusinsk Depression," in *Proceedings of Seminar on the Alkaline Magmatism of the Earth, Moscow, Russia, 2002* (Moscow, 2002), pp. 34–35 [in Russian].
31. R. H. Grapes, R. J. Wysoczanski, and P. W. O. Hoskin, "Rhonite Paragenesis in Pyroxenite Xenoliths, Mount Sidley Volcano, Marie Byrd Land, West Antarctica," Mineral. Mag. **67**, 639–651 (2003).
32. V. B. Naumov, V. I. Kovalenko, V. A. Dorofeeva, and V. V. Yarmolyuk, "Average Concentrations of Major, Volatile, and Trace Elements in Magmas of Various Geodynamic Settings," Geokhimiya, No. 10, 1113–1124 (2004) [Geochem. Int. **42**, 977–987 (2004)].
33. Yu. D. Litasov, V. G. Malkovets, K. D. Litasov, et al., "Petrogenesis of Basanites from the Pipes of the Northern Minusinsk Depression," in *Proceedings of Russian Foundation for Basic Research Conference Geology, Geochemistry, and Geophysics at the Turn of the 20th and 21th Centuries, Irkutsk, Russia, 2002* (Irkutsk, 2002), pp. 343–345 [in Russian].
34. R. Kerrich and D. A. Wyman, "Review of Developments in Trace-Element Fingerprinting of Geodynamic Settings and Their Implications for Mineral Exploration," Aust. J. Earth Sci. **44**, 465–487 (1997).
35. A. Zindler and S. R. Hart, "Chemical Geodynamics," Ann. Rev. Earth Planet. Sci. **14**, 493–571 (1986).
36. Yu. D. Litasov, "Evolution of the Alkali Basaltoids of Ingamakit and Munduzhyak Volcanoes, Udokan Lava Plateau," in *Thermobarogeochemistry of Mineral-Forming Processes* (OIGGM SO RAN, Novosibirsk, 1992), pp. 16–29 [in Russian].
37. G. Vaggelli, H. E. Belkin, and L. Francalanci, "Silicate-Melt Inclusions in the Mineral Phases of the Stromboli Volcanic Rocks: A Contribution to Understanding of Magmatic Processes," Acta Vulcanol. **3**, 115–125 (1993).
38. V. V. Sharygin, "Potassic Alkali Picrites of the Ryabinovyi Massif, Central Aldan," Geol. Geofiz. **34** (4), 60–70 (1993).
39. V. V. Sharygin and L. N. Pospelova, "Evolution of Melt during the Crystallization of Fergusite Porphyries, Eastern Pamirs," Geol. Geofiz. **35** (1), 110–117 (1994).
40. E. D. Andreeva, *Alkaline Magmatism of the Kuznetsk Alatau* (Nauka, Moscow, 1968) [in Russian].